ACS APPLIED NANO MATERIALS

www.acsanm.org Article

Nano-Capillary Bridges Control the Adhesion of Ice: Implications for Anti-Icing via Superhydrophobic Coatings

Ngoc N. Nguyen,* Sina Davani, Ramazan Asmatulu, Michael Kappl, Rüdiger Berger,* and Hans-Jürgen Butt

Cite This: *ACS Appl. Nano Mater.* 2022, 5, 19017−19024 Read Online

ACCESS | Metrics & More | Article Recommendations | Supporting Information

ABSTRACT: Understanding the ice adhesion mechanism is vital for efficient anti-icing. However, previous studies focused on the adhesion of already sintered ice-solid contacts. Here, we study the adhesion mechanism between preformed ice and solid surfaces. In particular, we investigate the initial stages of ice adhesion. We find that capillary bridges formed by the quasi-liquid layer on the ice surface enhance ice adhesion. The adhesion force showed a maximum around −2 °C. Our model indicates that the nano-scaled curvature of the capillary bridge gives rise to strong adhesion forces in the temperatures between −5 and 0 °C. The capillary bridge expands and consolidates over time, causing an increase of adhesion force. These findings provide new physical insights into the ice adhesion mechanism with strong implications to the development of water-repellent superhydrophobic coatings for efficient anti-icing of solid surfaces.

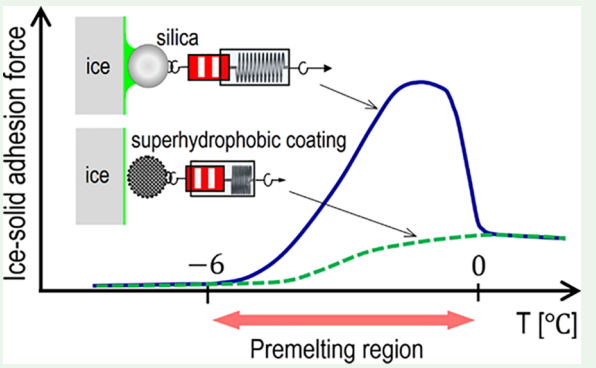

KEYWORDS: *ice adhesion, capillary attraction, quasi-liquid layer, surface premelting, superhydrophobic coating, adhesion force*

INTRODUCTION

Concerns related to ice adhesion are rising nowadays amid the rapid development of outdoor infrastructures. The adhesion of snow and/or ice on aircrafts leads to severe impacts on the safety and efficiency of aviation activities. Meanwhile, ongoing massive installations of wind turbines and solar panels, which amount to 1−2% of land areas in some countries,[1−3] are putting vast volumes of equipment surfaces into winter conditions and worsening the ice adhesion problems.[4,5] In all sectors, ice adhesion leads not only to reduced efficiency, imbalanced structures, power loss, and major disruptions in operations but also to significant risks of incidents.[4,5] For this reason, the adhesion of ice has been studied intensely,[6−9] even though previous studies dealt with the adhesion caused by freezing or frosting of water directly on solid substrates.[8−21] Frozen water binds to the solid substrates through an equilibrated ice-solid contact whose size and shape do not change with time. The adhesion force associated with such an equilibrated ice-solid interface was found to increase monotonically against lowering of the temperature.[13,14,22]

However, the ice adhesion in real-world systems can originate from the interactions between preformed ice particles, such as snow or hail, and solid surfaces. In this case, the preformed ice particles come to contact and interact with the solid substrate such as wind turbines, power lines, aircrafts, and so forth. The ice-solid contact may change with time owing to viscoelastic properties of the ice due to interfacial premelting and the formation of a quasi-liquid layer (QLL) on ice.[23,24] Hence, it is crucial to understand how the ice-solid contact changes after attachment and how it affects the adhesion force. Surprisingly, knowledge about the ice adhesion related to such a nonequilibrated ice-solid contact is elusive despite its scientific and practical significance.

Here, we explore the mechanism of the adhesion between ice and a solid surface concerning a nonequilibrium ice-solid contact regime. We measured and modeled the adhesion force between an ice surface and a solid sphere (radius, R = 0.8 mm) after they form a contact. The real-world ice adhesion usually involves ice particles interacting with solid surfaces. Here, we use the reverse model, solid particles interacting with an ice surface, because it is experimentally easier and the underlying physics is the same. It is challenging to prepare spherical ice particles, while silica spheres are commercially available. We demonstrate that the adhesion forces in these two models are mathematically identical (see Supporting Information). Hence, using the solid sphere−ice surface model makes the experiments more feasible, while ensuring the relevance of the

Received: November 10, 2022
Accepted: November 23, 2022
Published: December 13, 2022

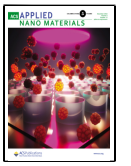

findings to the real-world ice adhesion problems. We focus on the initial phase within 10 min after ice-solid attachment to gain insights into dynamic ice-solid interactions, in particular, to answer the following questions: Can the ice-solid contact area change with time? What are the relevant length and time scales involved in such a change? Also, how does such dynamic nature of ice-solid contact affect ice adhesion? Our work reveals a new ice adhesion mechanism. The measured adhesion force shows a bell-shaped dependence on the temperature with a maximum force at a few minus degrees centigrade. This observation is interpreted using a model considering a microscopic capillary bridge formed by the QLL on the ice surface with the solid sphere. We demonstrate the dynamic feature of the ice-solid contact, showing that the contact is sustained by a microscopic capillary bridge between the ice and the solid sphere, which expands and consolidates in a time scale of minutes. This dynamic change of the ice-solid contact area is responsible for the increase of the adhesion force with time. By demonstrating that the ice adhesion is governed by capillary attraction, our findings and model provide the foundation for the development of water-repellent topologically rough hydrophobic coatings of surfaces for efficient anti-icing.

MATERIALS AND METHODS

Coatings of Silica Spheres. We used silica spheres of radius, R = 0.8 mm with a contact angle (θ) around 10° with water. To change wettability, different coatings were applied. Polymethyl methacrylate (PMMA) coating: Silica spheres were dip-coated in a solution of 1.0 wt % PMMA in tetrahydrofuran solvent (Sigma-Aldrich) for 1 min. After removing the sphere from the solution, it was annealed at 80 °C for 12 h in a vacuum oven to dry the PMMA film. The thickness of the PMMA film was 20 nm as measured by our profiler technique (KLA-Tencor Stylus-Profiler model P7). Teflon coating: Due to its low surface energy, Teflon is expected to have low adhesion.[25] Silica spheres were dip-coated in a solution of 4.0 wt % Teflon AF1600 in FC-43 solvent (Sigma-Aldrich) for 1 min. Then, the sphere with a film of Teflon was annealed at 160 °C for 12 h in a vacuum oven to dry the Teflon film. The thickness of the Teflon film was 400 nm as measured by our profiler technique.

Rough Hydrophobic Coating. A rough hydrophobic particle surface was created by coating silica microspheres to the 0.8 mm silica sphere. First, silica microspheres (mean diameter 10 μm, Bangs Laboratories Inc.) were dispersed in the aforementioned Teflon solution up to 5 wt % concentration (mass of microspheres per total mass of the suspension) by shaking and 30-min sonication. Then, the coating was implemented through the same dip-coating procedure as described for Teflon coating (Figure 1). A silica sphere (radius of 0.8 mm) was submerged into this suspension for 1 min. Upon slowly removing the silica sphere out from the suspension, a layer of microspheres remained on the surface. This coating layer was consolidated upon the evaporation of the solvent. The sample was annealed at 160 °C for 12 h to remove the solvent and improve the mechanical strength of the Teflon film. In this way, the macrosphere was coated with a more or less dense layer of microspheres (Figure 1).

Assessment of Surface Wettability. Since it is problematic to measure contact angles on the sphere, we measured the contact angles of water on glass slides that had coatings similar to each type of the aforementioned spheres. Using a commercial goniometer (Data-Physics), the contact angles for sessile drops were determined to be 70°, 115°, and 140° for PMMA coating, Teflon coating, and rough hydrophobic coating, respectively.

Measurements of Normal Adhesion Forces. We built a setup for measuring the normal adhesion force between an ice surface and a solid sphere. Details of this setup have been described in our previous paper.[26] Briefly, glass microcapillaries were used as mechanical force sensors (Figure S2).[27,28]

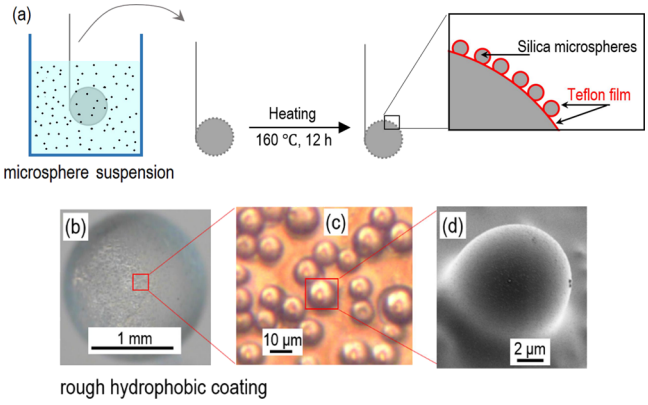

Figure 1. (a) Illustration of the dip-coating method for the preparation of the rough hydrophobic sphere. Teflon-coated microspheres were coated on the surface of the large sphere as micro hydrophobic protrusions to make the surface superhydrophobic-like. Optical microscopy images (b,c) and scanning electron microscopy image (d).

Each sphere was glued to the center of a capillary using epoxy glue (Figure 2). Having the sphere in the center position while allowing

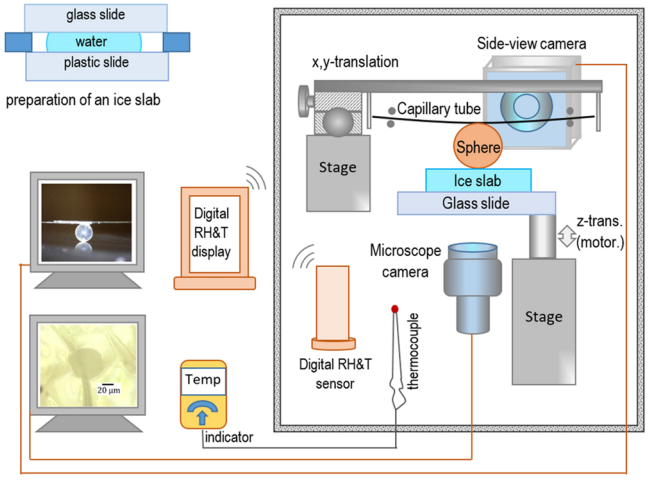

Figure 2. Experimental setup for measuring the normal adhesion force between a solid sphere and an ice surface. Adapted with permission from ref 26. Copyright, 2021, American Chemical Society.

both sides of the force sensor moving freely in a horizontal direction avoids any sliding motion of the sphere relatively to the ice surface. This improved feature provides a better accuracy of the measurement of the normal adhesion force[26] and is the key factor to detect the high adhesion force in the premelting region that might have been overlooked in previous studies. To prepare the ice surface, a volume (around 0.2 mL) of deionized water was confined in between two parallel slides, one was made of plastic and the other was made of glass. The water was then frozen. Then, the plastic slide was removed, leaving an ice slab with a thickness of 1 mm on the glass slide, which was used for the adhesion force measurement (Figure 2).

The x,y-translation makes it possible to measure the adhesion at different locations on the ice surface. A motorized z-translation stage engages the ice surface toward the sphere until it gently touches the sphere. After a defined contact time, the surface is withdrawn at a speed of 0.07 mm s^{-1}. The sphere sticks to the ice surface until the restoring force exerted by the force sensor overcomes the normal adhesion force. The normal adhesion force is determined in accordance with Hooke's law: $F = k \times \Delta x$. Stiff force sensors with spring constants (k) from 0.45 to 1.2 N m^{-1} were used for the original silica spheres and the PMMA-coated spheres. The minimal detectable

https://doi.org/10.1021/acsanm.2c04879
ACS Appl. Nano Mater. 2022, 5, 19017−19024

force was 3.5 μN. Softer force sensors (k= 0.026−0.110 N m^{-1}) were used for the Teflon-coated spheres and the rough hydrophobic spheres to better detect weak adhesion forces; the lowest detectable force in this case was 0.7 μN. For a given sensor, the spring constant could be changed by adjusting the distance between the two holders. Spring constants were measured by applying reference weights to the center point of the force sensors. The deflection of the force sensor in the center, Δx, was measured using a side-view camera.

Experiments were performed in a homebuilt "cold box" having an interior volume of 2 m^3 (Figure 2), which was created by modification of a big commercial freezer (GGM Gastro International). The sample and setup were handled with gastight gloves fixed to the transparent front side of the cold box. The temperature (T) and relative humidity (RH) were constantly monitored (KLIMALOGG Pro, TFA, accuracy of ±0.1 °C and ± 1%). The temperature is confirmed by a parallel measurement with a thermocouple (±0.1 °C) and a multimeter (EX505, Extech Instruments). For probing the contact area, a 0.3 mm thin ice slab was used for better transparency. The ice surface is brought to contact the sphere and the time-dependent contact area is captured by video microscopy (Olympus), as shown in Figure 2.

RESULTS

Adhesion Force versus Temperature. The normal adhesion forces between a pristine silica sphere (R = 0.8 mm) and an ice surface were measured against a stepwise increase of the temperature. For better comparison, we report a normalized adhesion force, which is the adhesion force divided by the radius of the sphere. The measured forces showed a "bell"-shaped dependence on the temperature (Figure 3). Three distinct temperature regimes can be distinguished. For temperatures below −6 °C, weak adhesion forces of roughly 0.05 N/m were observed. Between −6 and 0 °C, the adhesion forces increased by orders of magnitude before showing a sharp decrease. The maximum normalized force at −1 °C was typically 3 N/m. For temperatures >0 °C, the ice was melted, and the weak adhesion force was actually given by liquid water due to capillary attraction. This bell-shaped force versus temperature curve is specific for the adhesion involved non-equilibrated ice-solid contact since previous results on the equilibrated ice-solid interface showed a monotonic increase of adhesion force when lowering the temperature.[13,14,22]

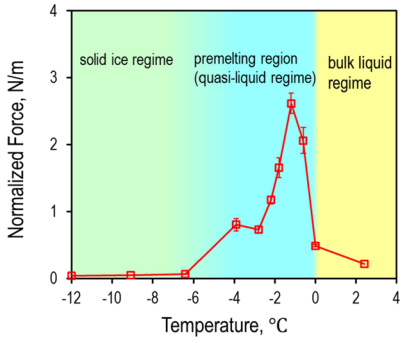

Figure 3. Bell shape of the force-versus-temperature curve measured for the normalized adhesion, F/R, between a pristine silica sphere and an ice surface. The adhesion force follows three distinct temperature-dependent regimes with a maximum in the premelting region. The silica sphere has a contact angle of around 10° with water. The contact time was 30 s.

We attribute the increase in adhesion force in the region between −6 and 0 °C to the occurrence of a QLL on the ice surface and the resulting capillary forces. The existence of a few nanometer-thick quasi-liquid or a liquid-like layer on ice is well established.[23,24,29−32] The temperature window for which such a QLL occurs significantly on ice coincides with the temperature range between −6 and 0 °C where we observed strong adhesion forces. For the temperatures lower than this range, the QLL might be discontinuous and does not have practical effects on the adhesion forces. For this reason, the temperature range between −6 and 0 °C is named here "premelting region." Van der Waals force is always present.

Van der Waals force for a sphere interacting with a plane is described by $F_{vdW} = {}^{A\times R}/_{6D^2}$, where R is the particle radius and D is the distance between the sphere and the surface.[33] When they are in contact, D corresponds to 0.16 nm. With A approximately equal to 3 × 10^{-20} J, we calculate F_{vdW} = 156 μN. The force normalized by particle radius is 0.2 N/m. This value is an upper limit because solid surfaces are never perfectly smooth. Typically, adhesion is dominated by asperities with a much lower radius of curvature. Hence, we neglected the contribution of van der Waals forces. The share of electrostatic forces in the premelting region is very small because the normalized forces are small at temperatures < −6 °C, where capillary forces are absent (Figure 3). Electrostatic forces do not depend on temperature. Therefore, in the premelting region, van der Waals and electrostatic forces are negligibly weak compared to capillary forces.

Elucidating Adhesion Mechanism. To explain the bell shape of the force-versus-temperature curves, we model the ice surface as having a nanometer-thick QLL on the top of a rigid solid ice (Figure 4a), similar to a thin liquid film on a solid substrate.[34,35] We assume that initially, the approaching sphere jumps through the QLL and displaces a volume of quasi-liquid equal to the volume of a spherical cap of height δ. Here, δ is the thickness of the QLL. The displaced liquid produces a microscopic meniscus in the form of a capillary bridge that induces a capillary force (F_{ca}) acting between the sphere and

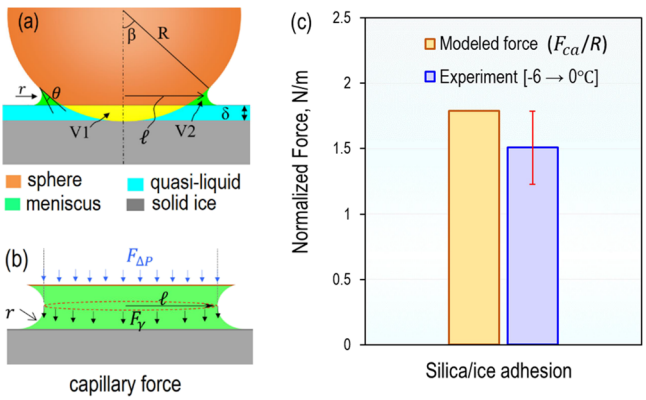

Figure 4. (a) Concepts of capillary bridge formation between a silica sphere and an ice surface upon contact. The QLL has a thickness δ forming a contact angle θ with the sphere. (b) Illustration of capillary force induced by the capillary bridge. (c) Comparison of the calculated capillary force with the averaged measured force. The normalized capillary force ($\frac{|F_{ca}|}{R}$; N m^{-1}) was calculated for R = 0.8 mm, δ = 10 nm, θ = 10°, and γ = 0.072 N m^{-1} based on eq 1. The experimental force is the average value of measured forces in the premelting region (between −6 and 0 °C) taken from the measurements shown in Figure 3, with a contact time of 30 s. Drawings are not to scales. (a) is adapted with permission from ref 26. Copyright, 2021, American Chemical Society.

https://doi.org/10.1021/acsanm.2c04879
ACS Appl. Nano Mater. 2022, 5, 19017−19024

the ice surface (Figure 4a,b). This force is the sum of the integral of the surface tension around the neck (F_γ) and the contribution of the Laplace pressure acting over the contact area ($F_{\Delta P}$),[36]

$$F_{ca} = F_\gamma + F_{\Delta P} = -2\pi\ell\gamma - \pi\ell^2\gamma\left(\frac{1}{r} - \frac{1}{\ell}\right) \quad (1)$$

Here, the minus sign indicates an attractive force. γ is the surface tension of the QLL. The radii of curvature ($\Delta P = -\gamma\left(\frac{1}{r} - \frac{1}{\ell}\right)$ and r, Figure 4a) can be expressed as a function of the contact angle θ of the quasi-liquid with the sphere.[26]

$$r = \frac{R(1 - \cos\beta) - \delta}{1 + \cos(\beta + \theta) + \sin\theta \times \sin\beta} \quad (2)$$

$$\ell = R\sin\beta - r(1 - \sin\beta) \quad (3)$$

We use δ = 10 nm as a typical value for temperatures of several minus degrees centigrade.[24,29,37] The surface tension γ of quasi-liquid is considered identical to that of water (0.072 N m^{-1}). The contact angle is θ = 10° for the silica surface. The filling angle β describes the position of the contact line, which can be determined by considering the volume of the quasi-liquid displaced by the spherical cap (V_1) is equal to the volume of the capillary neck (V_2).[26] For the aforementioned conditions, we obtained β = 0.4°. Substituting these parameters in eqs 1−3 enables the calculation of the capillary force (F_{ca}). The calculated capillary force was normalized ($|F_{ca}|/R$) and plotted together with the experimental force that is obtained by averaging the measured adhesion forces in the premelting region in Figure 3. The calculated capillary force (1.8 N m^{-1}) falls in the range of the averaged experimental force (1.5 ± 0.3 N m^{-1}) (Figure 4c). Hence, our model provides a good prediction of the normal adhesion force between the ice surface and the silica sphere.

Role of Surface Hydrophobicity. Applying our model to different contact angles enables the assessment of the effect of the surface hydrophobicity of the solid. The calculation shows that the adhesion force depends strongly on the contact angle θ of the QLL layer and the surface (Figure 5). The normalized capillary force decreases substantially upon the increase of the contact angle θ (the hydrophobicity) of the sphere from 1.79 N m^{-1} for a hydrophilic sphere with θ = 10° to 0.21 N m^{-1} for a superhydrophobic sphere with θ = 140° (Figure 5—blue curve). In order to experimentally verify our model, we tuned the surface hydrophobicity of the sphere by coating the original silica sphere. The measured adhesion forces follow the predicted trend (Figure 5—red data points). For the first three spheres including uncoated silica (10°), PMMA-coated (62°), and Teflon-coated (115°) ones, the differences between measured and calculated forces fall in the range of experimental errors (Figure 5).

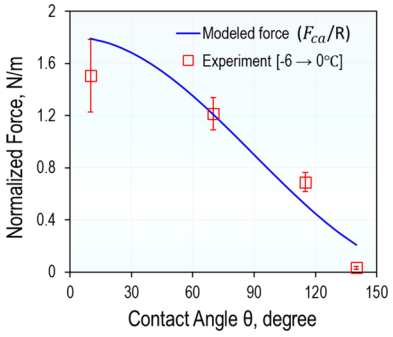

Figure 5. Normalized capillary force ($\frac{|F_{ca}|}{R}$; N m^{-1}) calculated from eq 1 for R = 0.8 mm, δ = 10 nm, and γ = 0.072 N m^{-1} and different contact angle values θ. Experimental forces were the average forces measured in the premelting region between −6 and 0 °C for the respective spheres, which were uncoated silica (10°), PMMA-coated (62°), Teflon-coated (115°), and rough hydrophobically coated sphere (140°). The contact time is 30 s.

Only the rough hydrophobically coated sphere (140°) showed an apparent discrepancy between the calculated (0.209 N m^{-1}) and measured (0.033 N m^{-1}) forces. This discrepancy is due to a fact that the modeled force (0.209 N m^{-1}) was based on a smooth hydrophobic sphere having a 0.8 mm radius and 140° contact angle, while the experimental force was measured using a rough hydrophobic sphere coated by 10 μm particles with an apparent contact angle of 140° (Figure 1). These microspheres as surface protrusions prevented the silica sphere from getting closer to the ice and reduced the contact area between the ice and the silica sphere and led to a reduced capillary attraction.

Now, we consider the contact area of the rough hydrophobic sphere with the ice sample to elucidate the origin of the reduced adhesion. This contact area is formed by only a few of the protruding microspheres. Therefore, the expected capillary force acting on the rough hydrophobic sphere can be calculated by applying our model in Figure 4a to individual microspheres contacting the QLL. The summed capillary force, normalized by the radius of the silica sphere (0.8 mm), varies in a range from 0.006 to 0.024 N m^{-1}, depending on the coverage (i.e., density) of the microspheres coated on the silica sphere. The details of this calculation are described in Figure S3. These calculated forces are in the same order of the measured force (0.033 N m^{-1}). Hence, the model agrees well with the experimental forces for both smooth and rough spheres and provides a universal description of the adhesion force between a solid sphere and an ice surface. In particular, a low adhesion force between ice and a rough hydrophobically coated surface would lead to the ice coming off the solid surface due to the gravity, vibration, wind, and/or hydrodynamic forces and enable anti-ice-adhesion performances.[38]

The "Bell-Shape Theory" of Ice Adhesion. The good agreement between experimental adhesion forces and modeling results indicates that capillary attraction by a QLL-induced capillary bridge dominates the interaction between the sphere and ice surface. For temperatures below the premelting region, the ice surface behaves similar to a typical solid. Hence, the ice adhesion at low temperatures is governed by van der Waals forces, leading to weak adhesion forces (Figure 3). For temperatures in the premelting region, the occurrence of the QLL leads to capillary attraction and the adhesion force increases accordingly. However, it is not straightforward to understand the reason behind the decrease of the adhesion force when the temperature increases further, yielding a bell shape of the force curve (Figure 3). In principle, the increase of the temperature would result in more quasi-liquid water on the ice surface.[24,29−32] The fact that the adhesion force decreases amid the increasing presence of quasi-liquid water is counter-intuitive.

We further analyze our model to explore the origin of the bell shape of the measured force-versus-temperature curves by decomposing the overall capillary force (F_{ca}) into a surface

https://doi.org/10.1021/acsanm.2c04879
ACS Appl. Nano Mater. 2022, 5, 19017−19024

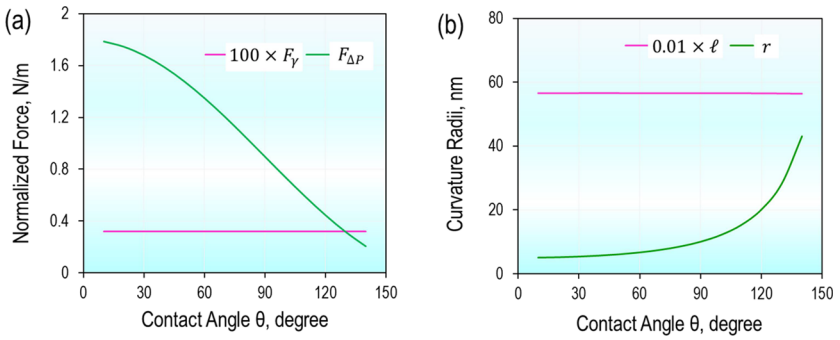

Figure 6. (a) Total capillary force (F_{ca}) is decomposed into Laplace pressure force ($F_{\Delta P}$) and surface tension force (F_γ) to reveal the dominating role of the $F_{\Delta P}$ in ice adhesion. (b) Radius (r) of curvature is nano-scaled, whereas the neck radius (ℓ) is micron-scaled. These parameters were calculated using eqs 1−3. The plots of F_γ and ℓ are scaled accordingly to fit the graphs.

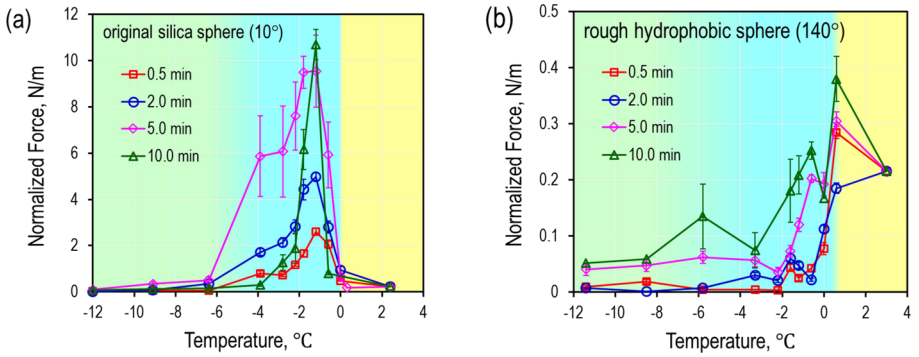

Figure 7. Time-dependent adhesion forces between an ice surface and the (a) silica and (b) rough hydrophobic spheres. The adhesion forces in (b) are orders of magnitude lower than that in (a), which demonstrates the effectiveness of rough hydrophobic coatings for the mitigation of ice adhesion.

tension force (F_γ) and a Laplace pressure force ($F_{\Delta P}$) in accordance with eq 1. We found that the Laplace pressure force far surpasses the surface tension force over the full range of contact angles and becomes a determining factor of the capillary attraction at the ice surface (Figure 6a). In addition, $F_{\Delta P}$ is sensitive to the hydrophobicity of the solid surface; it decreases from 1.79 N m^{-1} at θ = 10° to 0.26 N m^{-1} at θ = 140°. In contrast, F_γ is not sensitive to the solid surface; it decreases slightly from 3.2 × 10^{-3} N m^{-1} to 3.1 × 10^{-3} N m^{-1} corresponding to an increase of θ from 10° to 140°. Moreover, the radius r of curvature is nano-scaled and sensitive to the contact angle (Figure 6b). This radius increases strongly from 5 nm at θ = 10° to 43 nm at θ = 140°. In contrast, the neck radius ℓ is micron-scaled and not sensitive to the contact angle, showing a slight decrease from 5.6 μm at θ = 10° to 5.5 μm at θ = 140°. Figure 6a,b indicates that the increase of the radius r gives rise to a huge drop of Laplace pressure force. Thus, the nano-scaled radius (r) of curvature is the actual determining factor of the capillary force at the ice surface.

Now, the bell shape (Figure 3) can be fully explained. The decrease of adhesion force for the temperature range approaching the melting point of ice is due to a rapid thickening of the QLL.[24,29] Thicker QLL results in a larger radius (r) of the curvature that leads ultimately to the sharp decrease of the adhesion force. In particular, the adhesion forces measured in the melted region are given by a macroscopic capillary bridge between bulk liquid water and the respective spheres. Very large values of the radius r in this regime are the primary reason for low adhesion forces.

Dynamic Contact Area Yielding to Time-Dependent Adhesion Force. Experimental forces presented so far were measured for a short contact time of 30 s. During this short contact time, the formation of a microscopic capillary bridge dominates, and the measured adhesion force is fully described by the capillary force calculated by our model (Figure 5). The prerequisite for the validity of our model is the approximation that the displaced volume by the sphere jumping to contact is equal to the volume of the capillary meniscus, $V_1 \approx V_2$ in Figure 4a. However, adhesion forces increased with contact time (Figure 7) and exceeded the capillary force predicted by eq 1 for contact times longer than 30 s. Hence, it is important to understand the mechanism behind the time-dependent increase of the adhesion force.

We suggest that the increase in adhesion is caused by an expansion of the contact area. To experimentally confirm the time-dependent expansion of the contact area, we used optical microscopy from underneath the ice sample. Although the ice sample was only ≈0.3 mm thickness, the scattering of light reduces the quality of the captured images. Therefore, we binarized the optical images in order to extract the contact areas (Figure 8). The orange domains represent the contact area in binary images (Figure 8). Increasing the temperature leads to a larger contact area, which can be ascribed to the thickening of the QLL (vertical column in Figure 8). At a given temperature, the contact area expands with contact time (horizontal row in Figure 8). For short contact times within 1 min, the size of the contact areas falls in the same order of the modeled radius ℓ in Figure 6b.

https://doi.org/10.1021/acsanm.2c04879
ACS Appl. Nano Mater. 2022, 5, 19017−19024

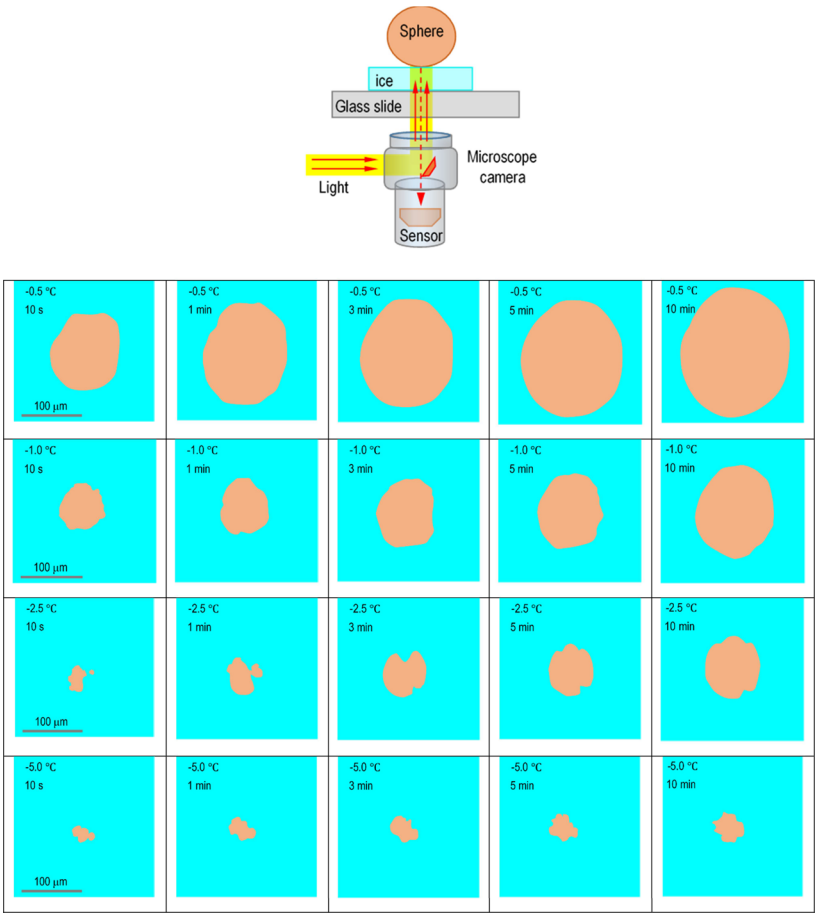

Figure 8. Expansion of the contact area (orange domains) between an original silica sphere (R = 0.8 mm) and an ice surface captured by a microscope camera positioned below the sample. Left to right is the increase of contact time at constant temperatures. Top to bottom is the decrease of the temperature at constant contact times. For low temperatures (below −5 °C), the ice surface behaves like a typical solid and no contact area could be observed by the microscope.

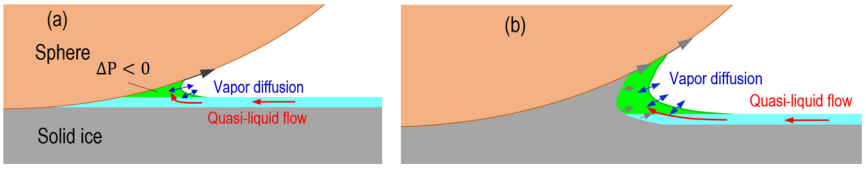

Figure 9. Model for the time-dependent expansion and consolidation (gray arrows) of the contact area between a solid sphere and an ice surface due to the flow of quasi-liquid (red arrows) and the vapor diffusion (blue arrows). (a) Large negative Laplace pressure drives quasi-liquid into the neck and causes the expansion of the contact area. (b) Additional formation of ice at the contact region consolidates the contact area and leads to a growing contribution of the consolidated ice-solid adhesion to the adhesion force. Drawings are not to be scaled.

Why does the contact area expand? We suggest that it is a transport by flow of the quasi-liquid-like layer and diffusion through the vapor phase. Both are driven by the concave shape of the meniscus. Both are coupled by fast condensation/evaporation equilibrium between the water vapor in the air gap and the quasi-liquid-like layer. In addition, the thickness of the quasi-liquid-like layer is stabilized by a solidification/melting equilibrium between the bulk ice and quasi-liquid-like layer. The driving force for liquid flow and vapor condensation is the highly concave curvature of the meniscus. The nano-scaled radius r of curvature causes a negative Laplace pressure in the neck. With the ranges of r and ℓ in Figure 6b and a surface tension approximately close to that of water (γ = 0.072 N m^{-1}), the theoretical Laplace pressure in the neck falls within a range between -0.9×10^5 and -1.4×10^7 Pa. Such large negative pressures draw additional quasi-liquid into the neck and cause the contact area expansion (Figure 9a,b). In addition, the curvature increases condensation because the local vapor pressure is reduced according to the Kelvin equation, with $P/P_0 = e^{\lambda(1/r - 1/l)}$ with the Kelvin length $\lambda = \gamma V_m/k_B T$. Here, P is the vapor pressure of water in equilibrium with the curved interface, P_0 is the saturation vapor pressure over a planar interface, V_m is the molecular volume of water, and k_B and T are Boltzmann's constant and temperature. With a Kelvin length of 0.53 nm for water, we find that the vapor pressure close to the meniscus is reduced by 0.07−11%. Therefore, the nature of the adhesion changes over time. For short contact time (within 1 min), the adhesion force is dominated by capillary attraction. For a longer contact time, the adhesion force is dominated by consolidated ice-solid

https://doi.org/10.1021/acsanm.2c04879
ACS Appl. Nano Mater. 2022, 5, 19017−19024

adhesion (Figure 9b). The latter leads to the time-dependent increase of experimental adhesion forces (Figure 7).

DISCUSSIONS

In contrast to the bell-shaped force-vs-temperature curves found by this work, previous results reported in the literature show that adhesion forces between ice and a solid surface monotonically increase with the decreasing temperature.[13,14,22] The reason for this discrepancy is that previous studies dealt with equilibrated ice-solid contacts where the ice specimens were formed directly on the solid surfaces via frosting or freezing.[8−21] In this case, the ice samples were already consolidated to the solid substrates (i.e., equilibrated contacts), and the size and shape of the contact areas do not change with time. However, not all ice adhesion problems originate from direct frosting or freezing of water on solid surfaces. In nature and industry, ice adhesion can arise from the interaction between preformed ice particles and solid surfaces, for example, the adhesion of snowflakes or hails on the surface of outdoor infrastructures. Our study of preformed ice samples coming to contact the solid surfaces advances the understanding of ice adhesion. Clearly, we demonstrated that the literature documented for equilibrated ice-solid contacts does not apply to nonequilibrated ice-solid interaction considered in this work.

The presence of QLL on the ice surface has been reported.[23,24,29−32,39] Therefore, one might anticipate a contribution of capillary attraction to ice-solid adhesion. However, it was thought to play only a minor role in ice adhesion forces. In addition, as the amount of quasi-liquid increases with the increase of the temperature,[23,24,29−32] one might expect that the adhesion force would increase continuously until the ice is melted because more quasi-liquid would favor the formation of capillary bridges. We ruled out this prejudice by revealing the maximum forces in the premelting region and figuring out the determining role of the curvature radius r of the capillary bridge. Thus, we established a "bell-shape" theory of ice adhesion. Therefore, nano-capillary bridges are able to control ice adhesion to a great extent. The observed force increase in the premelting region (between −6 and 0 °C) is of high practical importance since this temperature range is common in many countries. High adhesion forces in this ubiquitous temperature range favor the accretion of ice on solid surfaces.

Although our model and experiments deal with the interaction between a silica sphere and a flat ice surface, the findings are also relevant to the adhesion between an ice sphere and a solid surface since we demonstrate that the adhesion forces associated in the two models are mathematically identical (see Supporting Information). Moreover, the findings can be extended to the adhesion between an ice surface and a solid surface. The ice surface and the solid surface have inevitable roughness. Therefore, they form the contact through a number of surface asperities. At these contact points, the capillary bridges form and control the adhesion following the model that we have developed in Figure 4a,b.

CONCLUSIONS

We reported a new mechanism of ice adhesion involving preformed ice particles coming to contact with a solid surface. We revealed a bell-shaped dependence of the normal adhesion forces between the ice and solid substrate on the temperature and explained this adhesion behavior by considering the nano-capillary bridges formed between the QLL on the ice surface and the solid substrate. The finding of a strong adhesion force in the temperatures between −6 and 0 °C is of practical significance as this temperature range is ubiquitous in many countries in winter. Thus, nano-capillary bridges need to be considered in the development of anti-icing strategies. Our work provides new physical insights into the mechanism of ice adhesion. The findings have important implications for developing efficient anti-icing via adding a superhydrophobic coating to the solid surface.

ASSOCIATED CONTENT

Supporting Information

The Supporting Information is available free of charge at https://pubs.acs.org/doi/10.1021/acsanm.2c04879.

Comparison of two topological models of ice adhesion (ice sphere−solid surface and solid sphere−ice surface), description of force sensors used in this work, and estimation of the ice adhesion force with the rough hydrophobic surface (PDF)

AUTHOR INFORMATION

Corresponding Authors

Ngoc N. Nguyen − *Physics at Interfaces, Max Planck Institute for Polymer Research, 55128 Mainz, Germany;* Present Address: School of Chemical Engineering, The University of Queensland, St. Lucia, Brisbane, QLD 4072, Australia (N.N.N.); orcid.org/0000-0002-0999-1176; Email: n.nguyen9@uq.edu.au

Rüdiger Berger − *Physics at Interfaces, Max Planck Institute for Polymer Research, 55128 Mainz, Germany;* orcid.org/0000-0002-4084-0675; Email: berger@mpip-mainz.mpg.de

Authors

Sina Davani − *Mechanical Engineering Faculty, Wichita State University, Wichita, Kansas 67260, United States*

Ramazan Asmatulu − *Mechanical Engineering Faculty, Wichita State University, Wichita, Kansas 67260, United States*

Michael Kappl − *Physics at Interfaces, Max Planck Institute for Polymer Research, 55128 Mainz, Germany;* orcid.org/0000-0001-7335-1707

Hans-Jürgen Butt − *Physics at Interfaces, Max Planck Institute for Polymer Research, 55128 Mainz, Germany;* orcid.org/0000-0001-5391-2618

Complete contact information is available at: https://pubs.acs.org/10.1021/acsanm.2c04879

Funding

Open access funded by Max Planck Society.

Notes

The authors declare no competing financial interest.

ACKNOWLEDGMENTS

N.N.N. gratefully acknowledges the Alexander von Humboldt (AvH) Foundation for his AvH Fellowship for Postdoctoral Researchers (Fellowship Number: VNM 1200537 HFST-P). We acknowledge financial support by the German Research Society (DFG) via the Priority Programme 2171 Dynamic

wetting of flexible, adaptive, and switchable surfaces (BU 1556/36-1 and BE 3286/6-1). We thank Uwe Rietzler, Helma Burg, Xiaomei Li, and the mechanical and electronic workshops of MPIP for their technical assistance in building up the setup in a freezer.

REFERENCES

(1) Schulz, F. German Wind Industry Chief: 2% of Land Area Should Be Allocated to Wind Energy. https://www.euractiv.com/section/energy/interview/german-wind-industry-chief-2-of-land-area-should-be-allocated-to-wind-energy (accessed September 15, 2022)
(2) Ingram, E. Global Wind Industry to Deploy 1 TW of New Capacity through 2030. Renewable Energy World 2021. https://www.renewableenergyworld.com/wind-power/global-wind-industry-to-deploy-1-tw-of-new-capacity-through-2030/#gref (accessed September 15, 2022).
(3) Prakash, G.; Anuta, H.; Wagner, N.; Gallina, G. *Future of Wind: Deployment, Investment, Technology, Grid Integration and Socio-Economic Aspects*; International Renewable Energy Agency: Abu Dhabi, 2019; pp 1−88, https://www.irena.org/publications/2019/Oct/Future-of-wind (accessed November 22, 2022)
(4) Wallenius, T.; Lehtomäki, V. Overview of Cold Climate Wind Energy: Challenges, Solutions, and Future Needs. *Wiley Interdiscip. Rev.: Energy Environ.* **2016**, *5*, 128−135.
(5) Drapalik, M.; Zajicek, L.; Purker, S. Ice Aggregation and Ice Throw from Small Wind Turbines. *Cold Reg. Sci. Technol.* **2021**, *192*, No. 103399.
(6) Lv, J.; Song, Y.; Jiang, L.; Wang, J. Bio-Inspired Strategies for Anti-Icing. *ACS Nano* **2014**, *8*, 3152−3169.
(7) Bengaluru Subramanyam, S.; Kondrashov, V.; Rühe, J.; Varanasi, K. K. Low Ice Adhesion on Nano-Textured Superhydrophobic Surfaces under Supersaturated Conditions. *ACS Appl. Mater. Interfaces* **2016**, *8*, 12583−12587.
(8) Kreder, M. J.; Alvarenga, J.; Kim, P.; Aizenberg, J. Design of Anti-icing Surfaces: Smooth, Textured or Slippery? *Nat. Rev. Mater.* **2016**, *1*, 15003.
(9) Rønneberg, S.; He, J.; Zhang, Z. The Need for Standards in Low Ice Adhesion Surface Research: A Critical Review. *J. Adhes. Sci. Technol.* **2020**, *34*, 319−347.
(10) Boinovich, L. B.; Emelyanenko, K. A.; Emelyanenko, A. M. Superhydrophobic versus SLIPS: Temperature Dependence and the Stability of Ice Adhesion Strength. *J. Colloid Interface Sci.* **2022**, *606*, 556−566.
(11) Golovin, K.; Dhyani, A.; Thouless, M. D.; Tuteja, A. Low-Interfacial Toughness Materials for Effective Large-Scale Deicing. *Science* **2019**, *364*, 371−375.
(12) Martinsen, M.; Hed, K. O.; Diget, J. S.; Lein, H. L. A Novel Approach for the Evaluation of Ice Release Performance of Coatings Using Static Friction Measurements. *J. Coat. Technol. Res.* **2021**, *18*, 665−676.
(13) Work, A.; Lian, Y. A Critical Review of the Measurement of Ice Adhesion to Solid Substrates. *Prog. Aerosp. Sci.* **2018**, *98*, 1−26.
(14) Emelyanenko, K. A.; Emelyanenko, A. M.; Boinovich, L. B. Water and Ice Adhesion to Solid Surfaces: Common and Specific, the Impact of Temperature and Surface Wettability. *Coatings* **2020**, *10*, 648.
(15) Meuler, A. J.; Smith, J. D.; Varanasi, K. K.; Mabry, J. M.; McKinley, G. H.; Cohen, R. E. Relationships between Water Wettability and Ice Adhesion. *ACS Appl. Mater. Interfaces* **2010**, *2*, 3100−3110.
(16) Ling, E. J. Y.; Uong, V.; Renault-Crispo, J.-S.; Kietzig, A.-M.; Servio, P. Reducing Ice Adhesion on Nonsmooth Metallic Surfaces: Wettability and Topography Effects. *ACS Appl. Mater. Interfaces* **2016**, *8*, 8789−8800.
(17) Höhne, S.; Hoch, C.; Böhm, C.; Winkler, R.; Bittrich, E.; Uhlmann, P. A New Measuring System for the Determination of the Ice Adhesion Strength on Smooth Surfaces. *Langmuir* **2020**, *36*, 4465−4476.
(18) Lynch, F. T.; Khodadoust, A. Effects of Ice Accretions on Aircraft Aerodynamics. *Prog. Aerosp. Sci.* **2001**, *37*, 669−767.
(19) Capelli, A.; Reiweger, I.; Schweizer, J. Studying Snow Failure With Fiber Bundle Models. *Front. Phys.* **2020**, *8*, 236.
(20) Beeram, P. S. R.; Waldman, R. M.; Hu, H. *Measurements of Ice Adhesion over Ice Mitigation Coatings Pertinent to Aircraft Icing and Anti-/De-Icing*. In 9th AIAA Atmospheric and Space Environments Conference; 2017.
(21) Sojoudi, H.; Wang, M.; Boscher, N. D.; McKinley, G. H.; Gleason, K. K. Durable and Scalable Icephobic Surfaces: Similarities and Distinctions from Superhydrophobic Surfaces. *Soft Matter* **2016**, *12*, 1938−1963.
(22) Makkonen, L. Ice Adhesion-Theory, Measurements and Countermeasures. *J. Adhes. Sci. Technol.* **2012**, *26*, 413−445.
(23) Limmer, D. T. Closer Look at the Surface of Ice. *Proc. Natl. Acad. Sci. U. S. A.* **2016**, *113*, 12347−12349.
(24) Slater, B.; Michaelides, A. Surface Premelting of Water Ice. *Nat. Rev. Chem.* **2019**, *3*, 172−188.
(25) Drummond, C. J.; Georgaklis, G.; Chan, D. Y. C. Fluorocarbons: Surface Free Energies and van der Waals Interaction. *Langmuir* **1996**, *12*, 2617−2621.
(26) Nguyen, N. N.; Berger, R.; Kappl, M.; Butt, H.-J. Clathrate Adhesion Induced by Quasi-Liquid Layer. *J. Phys. Chem. C* **2021**, *125*, 21293−21300.
(27) Gao, N.; Geyer, F.; Pilat, D. W.; Wooh, S.; Vollmer, D.; Butt, H.-J.; Berger, R. How Drops Start Sliding over Solid Surfaces. *Nat. Phys.* **2018**, *14*, 191−196.
(28) Geyer, F.; D'Acunzi, M.; Sharifi-Aghili, A.; Saal, A.; Gao, N.; Kaltbeitzel, A.; Sloot, T.-F.; Berger, R.; Butt, H.-J.; Vollmer, D. When and How Self-cleaning of Superhydrophobic Surfaces Works. *Sci. Adv.* **2020**, *6*, 9727.
(29) Li, Y.; Somorjai, G. A. Surface Premelting of Ice. *J. Phys. Chem. C* **2007**, *111*, 9631−9637.
(30) Döppenschmidt, A.; Butt, H.-J. Measuring the Thickness of the Liquid-like Layer on Ice Surfaces with Atomic Force Microscopy. *Langmuir* **2000**, *16*, 6709−6714.
(31) Nagata, Y.; Hama, T.; Backus, E. H. G.; Mezger, M.; Bonn, D.; Bonn, M.; Sazaki, G. The Surface of Ice under Equilibrium and Nonequilibrium Conditions. *Acc. Chem. Res.* **2019**, *52*, 1006−1015.
(32) Sánchez, M. A.; Kling, T.; Ishiyama, T.; van Zadel, M.-J.; Bisson, P. J.; Mezger, M.; Jochum, M. N.; Cyran, J. D.; Smit, W. J.; Bakker, H. J.; Shultz, M. J.; Morita, A.; Donadio, D.; Nagata, Y.; Bonn, M.; Backus, E. H. G. Experimental and Theoretical Evidence for Bilayer-by-Bilayer Surface Melting of Crystalline Ice. *Proc. Natl. Acad. Sci. U. S. A.* **2017**, *114*, 227−232.
(33) Butt, H.-J.; Kappl, M. *Surface and Interfacial Forces*. Wiley-VCH Verlag GmbH & Co.: Weinheim, 2010, pp 1−423.
(34) Wang, Y.; Feng, Z.; Frechette, J. Dynamic Adhesion due to Fluid Infusion. *Curr. Opin. Colloid Interface Sci.* **2020**, *50*, No. 101397.
(35) Schellenberger, F.; Papadopoulos, P.; Kappl, M.; Weber, S. A. L.; Vollmer, D.; Butt, H.-J. Detaching Microparticles from a Liquid Surface. *Phys. Rev. Lett.* **2018**, *121*, No. 048002.
(36) Butt, H.-J. Capillary Forces: Influence of Roughness and Heterogeneity. *Langmuir* **2008**, *24*, 4715−4721.
(37) Nguyen, N. N.; Berger, R.; Butt, H.-J. Surface Premelting and Interfacial Interactions of Semi-Clathrate Hydrate. *J. Phys. Chem. C* **2019**, *123*, 24080−24086.
(38) Zhuo, Y.; Håkonsen, V.; He, Z.; Xiao, S.; He, J.; Zhang, Z. Enhancing the Mechanical Durability of Icephobic Surfaces by Introducing Autonomous Self-Healing Function. *ACS Appl. Mater. Interfaces* **2018**, *10*, 11972−11978.
(39) Nguyen, N. N.; Nguyen, C. V.; Nguyen, T. A. H.; Nguyen, A. V. Surface Science in the Research and Development of Hydrate-Based Sustainable Technologies. *ACS Sustainable Chem. Eng.* **2022**, *10*, 4041−4058.

https://doi.org/10.1021/acsanm.2c04879
ACS Appl. Nano Mater. 2022, 5, 19017−19024